



Mathematisch-Naturwissenschaftliche Fakultät

Safa Shoaee | Ardalan Armin | Martin Stolterfoht
Seyed Mehrdad Hosseini | Jona Kurpiers | Dieter Neher

Decoding Charge Recombination through Charge Generation in Organic Solar Cells

Suggested citation referring to the original publication:
Solar RRL (2019) Art. 1900184
DOI <https://doi.org/10.1002/solr.201900184>
ISSN (online) 2367-198X

Postprint archived at the Institutional Repository of the Potsdam University in:
Postprints der Universität Potsdam
Mathematisch-Naturwissenschaftliche Reihe ; 773
ISSN 1866-8372
<https://nbn-resolving.org/urn:nbn:de:kobv:517-opus4-437512>
DOI <https://doi.org/10.25932/publishup-43751>

Decoding Charge Recombination through Charge Generation in Organic Solar Cells

Safa Shoaee,* Ardalan Armin, Martin Stolterfoht, Seyed Mehrdad Hosseini, Jona Kurpiers, and Dieter Neher*

The in-depth understanding of charge carrier photogeneration and recombination mechanisms in organic solar cells is still an ongoing effort. In donor:acceptor (bulk) heterojunction organic solar cells, charge photogeneration and recombination are inter-related via the kinetics of charge transfer states—being singlet or triplet states. Although high-charge-photogeneration quantum yields are achieved in many donor:acceptor systems, only very few systems show significantly reduced bimolecular recombination relative to the rate of free carrier encounters, in low-mobility systems. This is a serious limitation for the industrialization of organic solar cells, in particular when aiming at thick active layers. Herein, a meta-analysis of the device performance of numerous bulk heterojunction organic solar cells is presented for which field-dependent photogeneration, charge carrier mobility, and fill factor are determined. Herein, a “spin-related factor” that is dependent on the ratio of back electron transfer of the triplet charge transfer (CT) states to the decay rate of the singlet CT states is introduced. It is shown that this factor links the recombination reduction factor to charge-generation efficiency. As a consequence, it is only in the systems with very efficient charge generation and very fast CT dissociation that free carrier recombination is strongly suppressed, regardless of the spin-related factor.

efficient free charge generation, which has subsequently led to the development of organic solar cells with power conversion efficiencies (PCEs) now reaching 16%.^[2–6] The ease of fabrication has always been the motivation behind OPV; however, the deposition of the typically thin active layer (<100 nm) over large areas using solution processing is challenging. This thickness limitation is mainly due to the short carrier lifetime relative to the transit time in disordered organic semiconductors. Recent high-efficiency devices underline that free carriers are readily generated within subnanosecond time scales of photoexcitation with a high efficiency independent of the internal electric field.^[7–9] The recombination mechanism in organic solar cells is apparently what occurs at longer time scales to the free carriers, i.e., nongeminate bimolecular recombination of charges. This recombination process with its associated rates is in competition with charge extraction (given by the internal electric field and typically poor charge carrier mobilities).

1. Introduction


Over the past years, organic photovoltaics (OPV) has evolved considerably. The introduction of the bulk heterojunction (BHJ) architecture^[1] allowed combining efficient exciton harvesting with

Therefore, it is intuitive to understand the nongeminate recombination loss as a voltage-dependent process. The fill factor (FF) that is the manifestation of the field dependence of all processes from charge generation to charge collection is believed to be the result of the aforementioned competition.^[10–12]

Because the charge extraction rate is thickness dependent, the recombination loss often scales with active layer thickness and remains as the primary loss factor in thick BHJ solar cells.^[13–16] It has been traditionally believed that in organic solar cells with much lower charge carrier mobilities compared with their inorganic counterparts, recombination can be regarded as a transport-controlled process, similar to that occurring in single-phase organic compounds or an ionized gas. This is expressed as Langevin-like recombination with a rate constant directly related to carrier mobilities. However, many systems exhibit reduced bimolecular recombination relative to the Langevin rate—beneficial for the operation of the cell in thick junctions. Yet, only very few material systems have shown a significant reduction.^[17–19] Material and device properties—including morphologic and energetic properties of organic semiconductors—have been examined to extend the Langevin model.^[20–22] Recently, several studies suggested that a highly reduced recombination cannot originate solely from the geometric confinement

Prof. S. Shoaee, Dr. M. Stolterfoht, S. M. Hosseini, Dr. J. Kurpiers, Prof. D. Neher
Optoelectronics of Disordered Semiconductors
Institute for Physics and Astronomy
University of Potsdam
14476 Potsdam-Golm, Germany
E-mail: shoai@uni-potsdam.de; neher@uni-potsdam.de

Dr. A. Armin
Department of Physics
Swansea University
Singleton Park, Swansea SA2 8PP, Wales, UK

 The ORCID identification number(s) for the author(s) of this article can be found under <https://doi.org/10.1002/solr.201900184>.

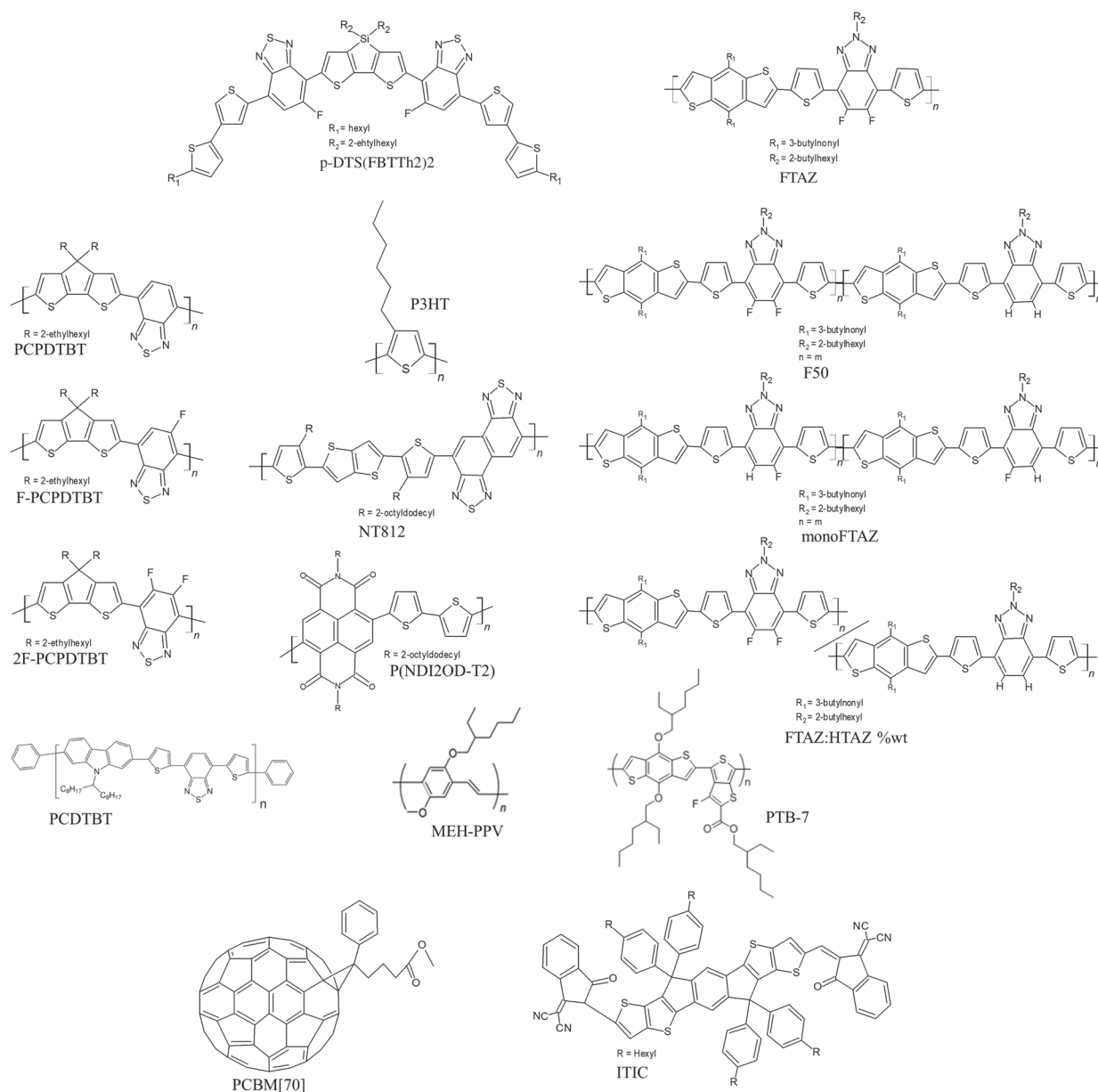
© 2019 The Authors. Published by WILEY-VCH Verlag GmbH & Co. KGaA, Weinheim. This is an open access article under the terms of the Creative Commons Attribution License, which permits use, distribution and reproduction in any medium, provided the original work is properly cited.

DOI: 10.1002/solr.201900184

of electrons and holes in their respective nanodomains,^[21] and any significantly reduced recombination should be related to the very efficient redissociation of charge transfer (CT) states (CTS).^[17,23,24] The basic idea behind the concept is that the encounter of free carriers causes the re-formation of CT states, meaning that fast dissociation of CT states lowers their steady-state density and thereby reduces the overall recombination via the CT decay to the ground state or to the triplet exciton states. Provided that the same manifold of CT states is involved in free charge formation and recombination, systems with strongly reduced recombination should also exhibit nearly perfect charge photogeneration. However, such a correlation cannot be directly observed from the internal quantum efficiency (IQE). This is mainly because IQE is affected not only by photogeneration

but also by the pseudo-first-order and second-order recombination of free charges. Therefore, establishing the most relevant physical model to relate recombination and photogeneration has remained a challenge to date, which demands for approaches to treat the competition between charge extraction and recombination of free carriers with respect to their photogeneration rate.

In this study, based upon new and previously published data, we analyzed over 20 donor:acceptor blend systems (chemical structures given in **Scheme 1**), using fullerene and nonfullerene acceptors blended with ten different donors, at different blend ratios and processing conditions—to study the role of charge-generation kinetics upon nongeminate recombination. We show for the first time how field-dependent charge generation, obtained from time-delayed collection field (TDCF), and the bimolecular recombination



Scheme 1. Chemical structure of the donors and acceptors studied in this work.

coefficient, obtained from bias-assisted charge extraction (BACE) at operating charge carrier densities, and mobilities (using space charge limited current [SCLC], resistance-dependent photovoltage [RPV], or TDCF) are related to one another and correlate with the FF. We will unify previous models for suppression of bimolecular recombination by introducing a “spin-related factor” that is dependent on the ratio of the back electron transfer rate of the triplet CT states to the decay rate of the singlet CTs. From the meta-analysis, it will be shown that geometrical confinement plays no role on the suppression of bimolecular recombination.

The work presents a satisfying understanding of the relation between field-dependent photogeneration, charge collection, and the FF. The results presented here, for the first time, visualize that efficient CT state dissociation as seen from field-independent photogeneration suppresses bimolecular recombination and increases the FF. Furthermore, we provide a model to explain the role of spin in the interplay between charge photogeneration and recombination in various donor:acceptor systems and introduce a spin-related factor that quantifies the relative strength of triplet and singlet CT state loss channels.

When the dissociation yield of excitons is nearly perfect, the charge generation efficiency can be approximated as the dissociation efficiency of the CT states

$$\eta_{CG} \approx \eta_{diss,CT} = \frac{k_d}{k_f + k_d} \quad (1)$$

in which k_d is the dissociation rate constant of the CT states to free charges and k_f the CT decay rate constant to the ground state. Assuming similar dissociation efficiency for both singlet (¹CT) and triplet CT (³CT) states, the free charge carrier generation rate is $k_d(n_{1CT} + n_{3CT})$, where n_{1CT} and n_{3CT} are carrier densities for singlet and triplet CT states, respectively. We note that triplet CT states can be generated via the intersystem crossing of singlet CT states^[25] or via encountering spin uncorrelated free electrons and holes.^[26]

At open-circuit and steady-state conditions, the net current is zero where the photocurrent is balanced out by the injection current. The kinetics of the charge carriers and the CT states can be written as

$$\frac{dn_{CS}}{dt} = -k_{en}n_{CS}^2 + k_d(n_{1CT} + n_{3CT}) = 0 \quad (2)$$

$$\frac{dn_{1CT}}{dt} = \frac{1}{4}k_{en}n_{CS}^2 - (k_d + k_f)n_{1CT} + k_{diss,EX}n_{1EX} - k_{ISC}(n_{1CT} - n_{3CT}) = 0 \quad (3)$$

$$\frac{dn_{3CT}}{dt} = \frac{3}{4}k_{en}n_{CS}^2 - (k_d + k_{BET})n_{3CT} + k_{ISC}(n_{1CT} - n_{3CT}) = 0 \quad (4)$$

where n_{CS} is the density of free carriers, k_{en} is the bimolecular encounter rate constant of free carriers with $k_{en}n_{CS}^2$ being the rate of regeneration of the CT states, and $k_{diss,EX}n_{1EX}$ is the rate at which singlet CT states are generated from excitons, which in ideal quenching condition equals the optical generation rate, G_{opt} . k_{BET} is the rate of back electron transfer (BET) of the triplet charge transfer (³CT) states to form triplet excitons on either the donor or acceptor, and k_{ISC} is the intersystem crossing (ISC) rate between the

singlet and triplet CTS. The fractions in Equations (3) and (4) come from spin statistics: there are three combinations of half spin that yield a triplet and one that results in a singlet. The encounter rate can be reduced for several reasons, one being due to geometrical confinement, as well as other morphological reasons^[27]—as such, all the different factors are termed together under the reduction term “ γ_{en} ,” taking into account any possible mechanism for lowering the encounter rate of the charge carriers. k_{en} can be written in terms of the geometrically reduced Langevin rate such that

$$k_{en} = \gamma_{en}k_L \quad (5)$$

where $k_L = (\mu_e + \mu_h)e/\epsilon\epsilon_0$ is the Langevin encounter rate and $\gamma_{en} (<1)$ the reduction factor due to the confinement of opposite charges in their nanodomains in a BHJ system. It is important to emphasize that all charge recombination occurs via CTS, so the recombination rate is given by the consideration of all loss channels and dead-ends, namely, the decay of the singlet CTS to the ground state and back electron transfer of the triplet CT states to triplet excitons. As such, the recombination rate to the ground state (R) is not simply given by $k_{en}n_{CS}^2$, as not all the re-formed CT states are dead-ends, due to CT redissociation. Rather, an effective bimolecular recombination coefficient, k_2 , of free carriers to the ground state is introduced, which is experimentally observable and defined by

$$R = k_f n_{1CT} + k_{BET} n_{3CT} \equiv k_2 n_{CS}^2 \quad (6)$$

where R is the total recombination rate of the re-formed singlet and triplet CT states. In general, k_2 can be related to the free charge encounter coefficient via $k_2 = \gamma_{CT}k_{en}$, yielding

$$k_2 = \gamma_{CT}\gamma_{en}k_L = \gamma k_L \quad (7)$$

where γ_{CT} is the CT recombination reduction factor and $\gamma = \gamma_{CT}\gamma_{en}$ the bimolecular recombination reduction factor.

Now let us consider the different conditions of CT state kinetics with the corresponding state diagram shown in **Figure 1**.

1.1. $k_d \ll k_f$ and k_{BET}

When CTS dissociation is much slower than the two loss rates (a very poor generation efficiency), the total recombination rate is entirely encounter limited and given by

$$R = k_2 n_{CS}^2 = k_{en} n_{CS}^2 = \gamma_{en} k_L n_{CS}^2 \quad (8)$$

In such a case, the total reduction factor relative to the Langevin rate is $\gamma = \gamma_{en}$, merely due to the geometrical confinement of the electrons and holes in their respective domains. It has been shown based on Monte Carlo simulations that in BHJ solar cells with domain sizes of less than 10 nm, this geometrical reduction can never be significant.^[21]

1.2. Fast Intersystem Crossing and Dissociation Rates:

$$k_{ISC} \gg k_{BET} \text{ and } k_d \gg k_f, k_d \gg k_{BET}$$

When the dissociation rate of CT states is much faster than the decay rate of ¹CT and back electron transfer rate of ³CT, the CT states are in equilibrium with free carriers, i.e., the chemical

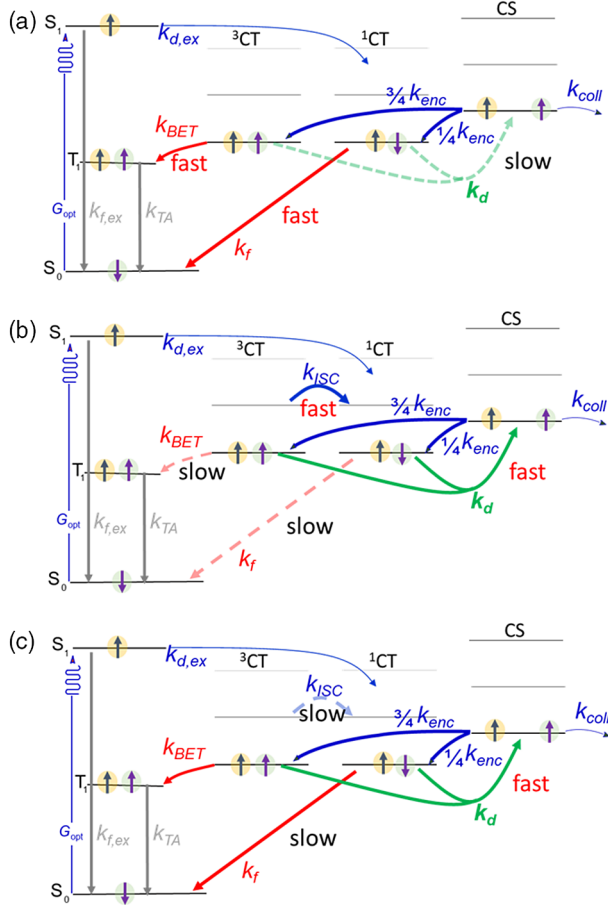


Figure 1. State diagram of BHJ solar cells for three different conditions of the CT state during a) poor charge generation, b) fast intersystem crossing and dissociation rates, and c) slow intersystem crossing and fast dissociation rates. The two main loss pathways of the CT states to the ground states are the decay of singlet CT states at the rate k_f to the ground state and the loss of the triplet CT states through back electron transfer to triplet excitons at rate k_{BET} .

potential of the CT states equals the quasi-Fermi-level splitting of the electrons and holes. The same scenario can happen even if k_d is not necessarily faster than k_{BET} but the intersystem crossing for ${}^3\text{CT} \rightarrow {}^1\text{CT}$ is very fast ($k_{\text{ISC}} \gg k_{\text{BET}}$). This will depopulate the triplet CT states and the kinetics is similar to the case where spin is neglected.

In this case of a fast dissociation rate, one can write

$$k_{\text{en}} n_{\text{CS}}^2 = k_d n_{\text{CT}} \quad (9)$$

where $n_{\text{CT}} = n_{1\text{CT}}$ due to ISC from ${}^3\text{CT}$ to ${}^1\text{CT}$. Then, recombination rate is

$$R = k_2 n_{\text{CS}}^2 = k_f n_{\text{CT}} = \frac{k_f}{k_d + k_f} k_{\text{en}} n_{\text{CS}}^2 = \gamma_{\text{CT}} \gamma_{\text{en}} k_L n_{\text{CS}}^2 \quad (10)$$

where we used the geometrically reduced encounter rate $k_{\text{en}} = \gamma_{\text{en}} k_L$. In the limiting case of a very small domain size, $\gamma_{\text{en}} \approx 1$, the reduction factor is

$$\gamma = \gamma_{\text{CT}} = \frac{k_f}{k_d + k_f} \quad (11)$$

Thereby, one can deduce a reverse correlation between the generation efficiency (Equation (1)) for steady-state recombination.

$$\gamma_{\text{CT}} = 1 - \eta_{\text{diss,CT}} \quad (12)$$

where $\eta_{\text{diss,CT}} = \frac{k_d}{k_d + k_f}$

Equation (1) is the efficiency of CT dissociation into free charges.

1.3. Slow Intersystem Crossing and Fast Dissociation Rates:

$k_d \gg k_f$ and $k_d \gg k_{\text{BET}}$

In this section, we consider the general case in which upon recombination of free carriers to CT states, a 1:3 ratio of singlet:triplet CTS is maintained. This is expressed as

$$k_{\text{en}} n_{\text{CS}}^2 = k_d (n_{1\text{CT}} + n_{3\text{CT}}) \quad (13)$$

and the recombination rate is given by

$$R = k_2 n_{\text{CS}}^2 = k_f n_{1\text{CT}} + k_{\text{BET}} n_{3\text{CT}} = \frac{k_f}{k_d + k_f} k_{\text{en}} n_{\text{CS}}^2 = \gamma_{\text{CT}} \gamma_{\text{en}} k_L n_{\text{CS}}^2 \quad (14)$$

where

$$\gamma_{\text{CT}} = \frac{\rho k_f}{\rho k_f + k_d} \quad (15)$$

in which

$$\rho = \frac{1}{4} + \frac{3 k_{\text{BET}}}{4 k_f} \quad (16)$$

We label parameter ρ as the “spin-related factor” that plays an important role in defining the regime of bimolecular recombination. When $k_{\text{BET}} = k_f$ ($\rho = 1$), the singlet and triplet states have the same loss kinetics and thereby “undistinguishable” in terms of their decay rate to the environment. In this regime, Equation (15) is reduced to Equation (11) in which the role of spin is ignored. When $k_{\text{BET}} \ll k_f$, $\rho = \frac{1}{4}$, and γ_{CT} will be defined by the ratio k_f/k_d , however, four times less than what is predicted when spin is neglected. When $k_{\text{BET}} \gg k_f$, ρ diverges and γ_{CT} will be dependent on the ratio of $\rho k_f/k_d$ and approaches 1 if $\rho k_f \gg k_d$.

Similar to Equation (12), we obtain an expression between reduction factor and charge-generation efficiency, but now taking spin into account.

$$\gamma_{\text{CT}} = \frac{\rho(1 - \eta_{\text{diss,CT}})}{\rho(1 - \eta_{\text{diss,CT}}) + \eta_{\text{diss,CT}}} \quad (17)$$

which yields Equation (12) when $\rho = 1$.

2. Experimental Results

We now turn to the consideration of experimental data to the extent to which the proposed variation in reduced recombination

can be correlated with variations in charge-generation efficiency. In this regard, we present a large amount of published and unpublished data from our own group and others, of over 20 systems (chemical structures shown in Scheme 1), where the field-dependent charge-generation efficiency, the recombination coefficient, and mobilities have been measured. Importantly, these systems are mostly characterized with same techniques, minimizing technique-related variations. Device performance characteristics are listed in Tables 1 and 2, Supporting Information (with exemplary TDCF, BACE, and mobility data for NT812:ITIC and NT812:PCBM[70] given in the Supporting Information). **Figure 2** shows *JV* curves for two model systems with and without a gradient of charge generation at short circuit under simulated 100 mW cm⁻² AM 1.5 G illumination, along with external generation efficiency (EGE) obtained from TDCF measurements, as described in studies by Hosseini et al. and Kurpiers and Neher.^[28,29] As discussed, both *JV* curves are well described by the estimated EGE at reverse bias, where recombination is reduced by the effect of the applied field. It is also evident that for the device with a gradient *JV* the effect of bias on generation is relatively large (EGE decreases by 25% from -2 V to *V*_{OC}), compared with the effect of the electric field on the EGE, which is very small in the other device (<5%). Generally, the EGE is determined in these systems as a function voltage and can be written as

$$\text{EGE}(V) = \text{IGE}(V) \times \eta_{\text{abs}} = \eta_{\text{diss,ex}} \eta_{\text{diss,CT}}(V) \eta_{\text{abs}} \quad (18)$$

where IGE is internal generation efficiency, η_{dissex} the exciton quenching yield, and η_{abs} absorption of the active layer. The latter two are nearly independent of the applied voltage.

To estimate $\eta_{\text{diss,CT}}(V_{\text{OC}})$ at open-circuit conditions [refer to Equations (12) and (17)], we normalized the experimentally determined external charge-generation efficiency at *V*_{OC} against the EGE at -2V at which in most cases a saturated photocurrent and EGE are achieved

$$\eta_{\text{diss,CT}}(V_{\text{OC}}) = \frac{\text{EGE}(V_{\text{OC}})}{\text{EGE}(J_{\text{sat}})} \quad (19)$$

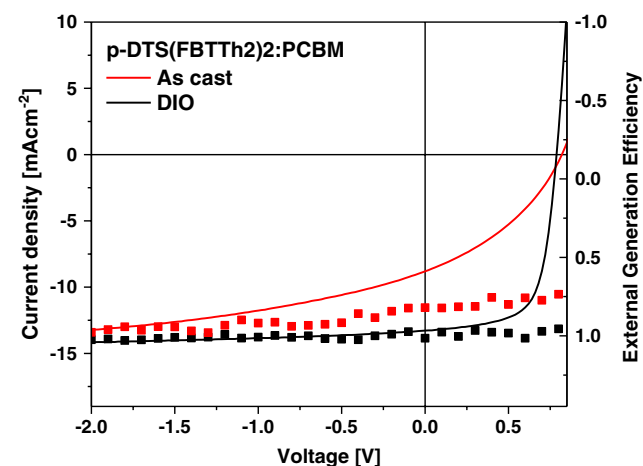


Figure 2. EGE and current density–voltage characteristics under simulated AM 1.5 G light calibrated to 100 mW cm⁻². Reproduced with permission.^[13] Copyright 2013, Wiley-VCH.

This normalization ensures that imperfect exciton quenching, light reflection, and parasitic absorption by nonactive layers are ruled out and $\eta_{\text{diss,CT}}(V_{\text{OC}})$ is a direct indicator of efficiency of dissociation of initially generated interfacial polaron pairs into dissociated charges.

To relate the efficiency of charge generation at *V*_{OC} with recombination, we used steady-state BACE to measure the recombination rate *k*₂ under steady-state illumination at *V*_{OC}. Furthermore, the carrier mobility for each system has also been measured—under device operational conditions when carriers have been thermalized—to calculate *k*₁; all values are presented in Table 2, Supporting Information. **Figure 3** shows the correlation between this assay of $\eta_{\text{diss,CT}}$ and reduced recombination of free carriers, as presented in Equation (12). The reduction factor γ was estimated from dividing the experimentally measured bimolecular recombination rate constant by the inferred Langevin rate from experimentally measured electron and hole mobilities.

For all systems presented in Figure 3, a good correlation is observed between $\eta_{\text{diss,CT}}$ and its corresponding bimolecular recombination reduction factor, whereby we observe the reduction factor decreasing (recombination becoming slower) with increasing charge-generation efficiency. When charge generation is field independent ($\eta_{\text{diss,CT}} > 95\%$), strongly reduced recombination is heuristically achieved. However, at lower $\eta_{\text{diss,CT}}$ when charge generation is field dependent, pointing to a small dissociation rate *k*_d, encounter-limited recombination or very modestly reduced recombination is observed, as predicted by Equation (17). In contrast, there are some systems that exhibit a quite efficient generation, however, with a fairly large γ , implying recombination proceeds mostly through back electron transfer. The dashed lines which are fits to Equation (17) show different values of ρ . Most systems lie on $\rho = 0.4 - 1$, suggesting a *k*_{BET}/*k*_f ratio between 0.2 and 1.0. The most efficient system

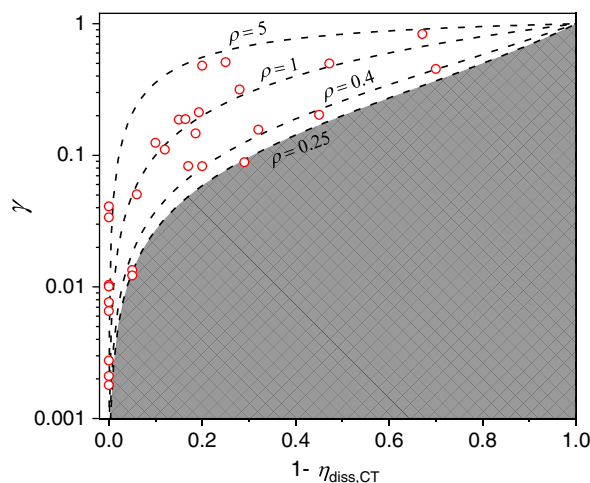


Figure 3. Correlation of data from Table 1, Supporting Information, between γ (bimolecular recombination reduction factor) and the CT state dissociation efficiency, $\eta_{\text{diss,CT}}$ under operational conditions. The dashed lines represent Equation (17) for different values of the spin-related factor ρ . The absence of data points below the $\rho = 0.25$ line indicates that geometrical confinement plays no role in the suppression of bimolecular recombination such that $\gamma = \gamma_{\text{CT}}$ in the 24 systems studied herein.

with strongly reduced recombination has $\rho = 0.25$, indicating negligible back electron transfer. This model showcases the importance of suppressing the triplet loss channel to achieve reduced recombination and efficient charge generation. Notably, none of the data points lie below the $\rho = 0.25$ line. As $\gamma = \gamma_{CT}\gamma_{en}$ refers to the Langevin recombination rate, the absence of data points below this line implies that reduced recombination stems almost entirely from the dissociation of re-formed CT states (expressed by $\gamma_{CT} < 1$) and that the reduced encounter rate of free carriers plays an insignificant role in the reduction of bimolecular recombination (i.e., $\gamma_{en} \cong 1$) in most of the studied blends.

3. Limitations and Outlook of the Model

Our model represents a general frame for the relationship between charge generation and the Langevin reduction factor, which has the assumption that the rate of dissociation of the CT state formed through photogenerated carriers and that formed due to the encountering of free carriers through space are proportional. The model should be refined for the system in which the hot CT state or delocalization determines the rate of photogenerated CT state dissociation involving charge generation. Yet, this should only affect the systems with high charge-generation efficiency. The additional shortcomings of our model come from the experimental limitation in determining the exact charge-generation yield in systems with nearly unity quantum yields. This is not only a limitation of the methodology we used but a problem that the community has not yet overcome: how to detect near-unity charge-generation quantum yield. The technical limitation is mainly due to the variations in the TDCF data versus the voltage that arises from laser fluctuations and uncertainty of the extracted charges evaluated by the integration of the current transients as well as the very precise determination of the number of photons. As such, our experimental methodology is not able to quantitatively explain systems above 99% quantum yield. However, and given this limitation, even in these systems, the expected trend as shown by the dashed lines in Figure 3 is still observable, that is, the larger the charge-generation quantum yields, the smaller the reduction factor.

4. Interrelation between the Efficiency of CT Dissociation and the Fill Factor

We now turn to the consideration of the FF by focusing on the same material systems as mentioned earlier. FF is a sensitive parameter as it summarizes all field-dependent processes. As such, it depends not only on the CT dissociation efficiency, the electron and hole mobilities, the recombination coefficient but also the thickness of the active layer. For high-mobility materials, the current voltage characteristics are given by the Shockley diode equation, and the FF is a sole function of the V_{oc} , the ideality factor, and the temperature. Recently, Neher et al. reported a modified Shockley equation, which takes into account transport limitations in organic solar cells due to low mobilities.^[10] If free charge generation is independent of bias, the model also allows to predict the FF from a unit-less parameter, $\alpha = \left(\frac{qk_2d^3J_G}{4\mu_h\mu_e(kT)^2}\right)^{1/2}$,

which contains information on the transport and recombination properties of the active layer such that d is the active layer thickness, k the Boltzmann constant, T the absolute temperature, and J_G generation current. Here, we have evaluated generation current from the saturated photocurrent. Figure 4a demonstrates the experimentally determined FFs at AM1.5 G illumination for various systems as a function of α , based upon the modified Shockley equation (the black rectangles). Also plotted on the same figure is the calculated values of the FF for each system based on the approach presented by Neher et al.^[10] (red circles) figure of merit model. Although the model predicts the overall FF trend, there is a large spread observed in the experimental FF data. In particular, the prediction overestimates the FF for systems exhibiting field-dependent charge generation, which is reasonable as the model neglects any field dependence of free charge generation. However, recent studies reported voltage-dependent charge photogeneration in BHJ solar cells and discussed the impact of this on the device's FF.^[30,31] In fact, several of the blend systems in Table 1, Supporting Information, reveal field-dependent charge generation. In this regard, we correct the measured FF data to take account of the variations in field dependence by defining

$$FF_{corrected} = \frac{FF - FF_0(1 - EGE)}{EGE} \quad (20)$$

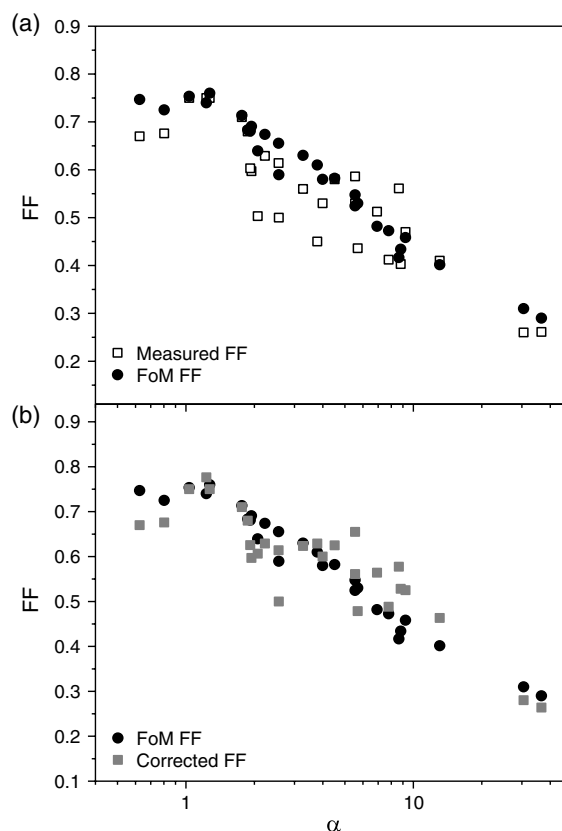


Figure 4. Theoretically predicted FF as a function of alpha based upon the modified Shockley diode equation given in the citation,^[9] together with a) experimentally measured FFs and b) the measured FF from (a), normalized for field-dependent charge generation.

where FF is the measured value and FF_0 is a value that corresponds to a linear JV profile in the power-generating quadrant (i.e., $FF = 0.25$): in the limiting case of poor charge generation, the photocurrent is determined by the field dependence of generation, which is assumed to be linearly dependent on voltage. In contrast, when charge generation is field independent ($EGE = 1$), $FF_{corrected} = FF$. As such by correcting the measured FF values by field-dependent charge-generation efficiency (Equation (20)) to yield the upper limit for FF, as shown in Figure 4b, we observe a better agreement between the calculated and the measured values (corrected for field dependence). For each system, the FF predicted by the model of Neher et al. (red rectangles in Figure 4) is the upper limit of the FF, which can be achieved if charge generation for that given system is independent of the electric field. The remaining data spread can be due to series and shunt resistances, which are not considered in the model.

Following the aforementioned discussions, when k_d is large enough already at zero field, and consequently the CT splitting proceeds at a higher rate than their recombination, it results in a very efficient charge-generation quantum yield even under open-circuit conditions. Thereby, field-independent efficient charge generation is expected. Thus, it is clear that within this model, a key kinetic competition in achieving high FF is between the dissociation of the CT state and loss decays of the CT states (when $k_d \gg k_f + k_{BET}$). This emphasizes the importance and influence of field-dependent charge generation on the FF; in systems where charge collection is inefficient due to significant recombination (encountered limited), the FF is not only governed by the direct field dependence of first-order charge generation but also the competition between charge extraction and bimolecular recombination due to the lower dissociation rate of the CT state, which itself also causes field-dependent charge generation.

In conclusion, we have investigated the generality of the previously hypothesized explanation on reduced recombination for numerous different systems and have shown for the first time correlations between field-dependent charge-generation efficiency and reduction of bimolecular recombination, taking into account the effect of spin. We introduced a “spin-related factor” that quantifies the kinetics of singlet and triplet CT states. The results reported in this article provides strong evidence that a key factor determining bimolecular recombination efficiency of photogenerated carriers and the FF is the efficiency of charge generation, where the key kinetic competition in suppressing the recombination is between dissociation of the CT state and loss decays of the CT states such that that charge-neutral molecules in their ground state are restored. The experimental data are rationalized by appreciating how the CT state mediates the interplay between charge generation and bimolecular recombination. Our results also indicated that the geometric confinement of the holes in the donor domains and electrons in acceptor domains plays an insignificant role in the suppression of bimolecular recombination. In addition, we have shown that the FF can suffer from inefficient generation in two ways: 1) charge generation itself being field dependent and subsequently 2) poor generation efficiency (i.e., field dependent), causing a less suppressed bimolecular recombination, therefore, a higher k_2 . Our results indicate that to reduce bimolecular recombination significantly with respect to the diffusion-limited encounter rate of the charge carriers, and

achieve FF close to the upper theoretical limit, one needs to suppress the loss channels from both singlet and triplet CT states simultaneously. This can be elegantly achieved by increasing the CT state’s dissociation rate to free carriers and obtaining field-independent generation efficiencies of 100%. While the origin of this rate concept is beyond the scope of this article, we anticipate that crystallinity, domain purity, and effectively local mobility play important roles in determining the rate of k_d .

5. Experimental Section

Solar-cell fabrication and characterization: Most data points used in this study were taken from previous published works. Few new systems were also used including NT812:PCBM[70], NT812:ITIC, MEH:PPV, P3HT:PCBM, and PTB7:PCBM[70]. For these systems, prepatterned indium tin oxide (ITO)–glass substrates were precleaned successively with detergent, acetone, deionized (DI) water, and IPA and dried by nitrogen. The dried substrates were treated by oxygen plasma at room temperature for 4 min and then coated with PEDOT:PSS by spin coating (3000 rpm for 30 s, thickness of ≈ 40 nm) and were then baked at 150°C for 15 min in air. For the deposition of active layers, the blend solution of the polymer (NT812 with polydispersity index $PDI \approx 2$) with PCBM[70] or ITIC at different weight ratios was dissolved in chlorobenzene:dichlorobenzene = 3:1 (with 0.5 vol% of 1-chloronaphthalene) and the blend solution of polymer:ITIC at different weight ratios was dissolved in *o*-xylene (with 1 vol% of 1-methyl-2-pyrrolidinone) and spin coated on top of the PEDOT:PSS layer in a nitrogen-filled glove box. Typically, an active layer of 100 nm thickness was achieved using polymer concentrations of 4 and 9 mg mL^{-1} for NT812:PCBM[70] and NT812:ITIC, respectively. Thermal annealing of the blend films was carried out by placing the films on a hot plate at 100°C for 15 min and 160°C for 20 min for NT812:PCBM[70] and NT812:ITIC, respectively, in a nitrogen atmosphere. A 5 nm-PFN-Br layer was then spin coated from the methanol solution onto the active layers.

To fabricate the PTB-7:PCBM active layers, PTB-7 and PCBM were separately dissolved in 1,8-diiodooctane (DIO):chlorobenzene (3:97 vol%) and then mixed to different blend ratios (by weight) with a total concentration of 25 g L^{-1} and subsequently spin coated at 1000 rpm, yielding an active layer thickness of 100 nm.

For the P3HT:PC60BM devices, 30 mg of PC60BM was dissolved in 1 mL of DCB at 70°C and then stirred at room temperature overnight. The PC60BM solution was then filtered before adding 30 mg of P3HT, and the final mixture was left on the hot plate at 70°C for 1 h. The blend solution was spin coated once it was cooled down to room temperature within ≈ 15 min. 90 nm-thick films were deposited by spin coating 15 mg mL^{-1} solutions at 600 rpm and subjected to solvent annealing overnight. After top electrode evaporation, the device was thermally annealed for 2 min at 170°C .

The blend of MEH-PPV:PCBM (1:4 by weight ratio with a total concentration of 25 mg) in the chlorobenzene solution was spin coated at 800 rpm for 50 s, yielding an active layer thickness of 100 nm.

The thin films were transferred into a vacuum evaporator connected to a glove box, and Ag (100 nm for the NT812 devices), Al (100 nm for P3HT:PCBM), and LiF/Al (0.8 and 100 nm for MEH-PPV) were deposited sequentially through a shadow mask under $\approx 1 \times 10^{-7}$ mbar, with an active area of the cells, of $A = 0.011\text{ cm}^2$, for BACE and TDCF measurements, and $A = 0.06\text{ cm}^2$ for JV measurement.

UV-visible absorption and photoluminescence spectroscopy: UV-visible spectra of the thin films were acquired with the Cary 5000 UV-Vis-NIR spectrophotometer in air. The photoluminescence (PL) spectra were measured with a Fluorolog-3 spectrofluorometer (Horiba Jobin Yvon). All film samples were spin coated on glass substrates. UV-vis and PL were used to determine excitation wavelengths as well as document the crude morphology as reflected in absorption and PL.

Time-Delayed Collection Field: In the TDCF experiment, a laser pulse from a diode-pumped, Q-switched Nd:YAG laser (NT242, EKSPILA) with 6 ns pulse duration and a typical repetition rate of 500 Hz working at

532 nm was used to generate charges in the device. A pulse generator (Agilent 81150A) was used to apply the pre- and collection biases that were amplified by a home-built amplifier. The current through the device was measured via a grounded 10 Ω resistor in series with the sample and with a differential current probe recorded with an oscilloscope (DSO9104H). The pulse generator was triggered with a fast photodiode (EOT, ET-2030TTL). The fluence was determined with a CCD camera in combination with a calibrated photodiode sensor (Ophir) and a laser-cut high-precision shadow mask to define the illuminated area.

Bias-assisted charge extraction: The experimental setup required for BACE measurements was similar to the TDCF setup, except for the illumination conditions. The steady-state condition was established by a high-power, 1 W, 638 nm laser diode (insaneware) with a switch-off time of about 10 ns. The light-emitting diode (LED) was operated at 500 Hz with a duty cycle of at least 50% of one period, which means 1 ms of illumination before the diode was switched off for 1 ms. After switching off the laser diode, a high reverse bias was applied and all charges were extracted. The fast switch-off time of the diode and the fast pulse generator (Agilent 81150A) allowed for charge extraction as fast as 10–20 ns after the switch off. The current transients were measured via a grounded 10 Ω resistor and recorded with an oscilloscope (DSO9104H) in the same way as that of the TDCF measurement.

Resistance-dependent photovoltage: Photocurrent and photovoltage transients were recorded using a digital storage oscilloscope (DSO9104H) via a LabVIEW code. A pulsed second-harmonic Nd:YAG laser (NT242, EKSPLA) working at 450 nm was used with 6 ns pulse duration. The laser beam with ≈50 mJ energy output was attenuated with a natural optical-density (OD) filter set. Low laser pulse fluences (≈OD 7) were used for the RPV mobility measurements to prevent the redistribution (screening) of the internal electric field, maintaining quasi-short-circuit conditions regardless of load resistance.

Space charge limited current: Electrical measurements were carried out on devices fabricated using ITO/PEDOT:PSS/active layer/MoO₃/Au for hole-only and ITO/Ca/active layer/PFN/Al for electron-only devices with NT812:PCBM[70] and NT812:ITIC as the BHJ active layers.

Supporting Information

Supporting Information is available from the Wiley Online Library or from the author.

Acknowledgements

Thanks to the Alexander von Humboldt Foundation for funding. A.A. acknowledges support by the Sêr Cymru Program through the European Regional Development Fund, Welsh European Funding Office, and Swansea University strategic initiative in Sustainable Advanced Materials.

Conflict of Interest

The authors declare no conflict of interest.

Keywords

charge generation, charge transfers, non-Langevin recombination, spin-related factors

Received: May 9, 2019

Revised: July 18, 2019

Published online:

- [1] G. Yu, J. Gao, J. C. Hummelen, F. Wudl, A. J. Heeger, *Science* **1995**, 270, 1789.
- [2] W. Zhao, S. Li, H. Yao, S. Zhang, Y. Zhang, B. Yang, J. Hou, *J. Am. Chem. Soc.* **2017**, 139, 7148.
- [3] D. Baran, N. Gasparini, A. Wadsworth, C. H. Tan, N. Wehbe, X. Song, Z. Hamid, W. Zhang, M. Neophytou, T. Kirchartz, C. J. Brabec, J. R. Durrant, I. McCulloch, *Nat. Commun.* **2018**, 9, 1.
- [4] S. Zhang, Y. Qin, J. Zhu, J. Hou, *Adv. Mater.* **2018**, 30, 1.
- [5] J. Yuan, Y. Zhang, J. Yuan, Y. Zhang, L. Zhou, G. Zhang, H. Yip, T. Lau, X. Lu, Y. Li, Y. Zou, *Joule* **2019**, 3, 1140.
- [6] Y. Cui, H. Yao, J. Zhang, T. Zhang, Y. Wang, L. Hong, K. Xian, B. Xu, S. Zhang, J. Peng, Z. Wei, F. Gao, J. Hou, *Nat. Commun.* **2019**, 10, 2515.
- [7] F. Etzold, I. A. Howard, R. Mauer, M. Meister, T.-D. Kim, K.-S. Lee, N. S. Baek, F. Laquai, *J. Am. Chem. Soc.* **2011**, 133, 9469.
- [8] S. Shoaee, F. Deledalle, P. S. Tuladhar, R. Shivanna, S. Rajaram, K. S. Narayan, J. R. Durrant, *J. Phys. Chem. Lett.* **2015**, 6, 201.
- [9] A. A. Bakulin, A. Rao, V. G. Pavelyev, P. H. M. van Loosdrecht, M. S. Pshenichnikov, D. Niedzialek, J. Cornil, D. Beljonne, R. H. Friend, *Science* **2012**, 335, 1340.
- [10] D. Neher, J. Kniepert, A. Elimelech, L. J. A. Koster, *Sci. Rep.* **2016**, 6, 1.
- [11] I. d. C. Pérez D. Bartesaghi J. Kniepert, S. Roland, M. Turbiez, D. Neher L. J. A. Koster, *Nat. Commun.* **2015**, 6, 1.
- [12] A. Yamacyan, M. Stolterfoht, P. L. Burn, Q. Lin, P. Meredith, A. Armin, *Adv. Energy Mater.* **2018**, 8, 170339.
- [13] C. M. Proctor, C. Kim, D. Neher, T. Q. Nguyen, *Adv. Funct. Mater.* **2013**, 23, 3584.
- [14] A. Maurano, R. Hamilton, C. G. Shuttle, A. M. Ballantyne, J. Nelson, B. O'Regan, W. Zhang, I. McCulloch, H. Azimi, M. Morana, C. J. Brabec, J. R. Durrant, *Adv. Mater.* **2010**, 22, 4987.
- [15] D. Credgington, R. Hamilton, P. Atienzar, J. Nelson, J. R. Durrant, *Adv. Funct. Mater.* **2011**, 21, 2744.
- [16] C. Göhler, A. Wagenpfahl, C. Deibel, *Adv. Electron. Mater.* **2018**, 1700505, 1.
- [17] A. Armin, J. Subbiah, M. Stolterfoht, S. Shoaee, Z. Xiao, S. Lu, D. J. Jones, P. Meredith, *Adv. Energy Mater.* **2016**, 6, 1600939.
- [18] A. Armin, Z. Chen, Y. Jin, K. Zhang, F. Huang, S. Shoaee, *Adv. Energy Mater.* **2017**, 8, 1701450.
- [19] N. Gasparini, M. Salvador, T. Heumueller, M. Richter, A. Classen, S. Shrestha, G. J. Matt, S. Holliday, S. Strohm, H. J. Egelhaaf, A. Wadsworth, D. Baran, I. McCulloch, C. J. Brabec, *Adv. Energy Mater.* **2017**, 1701561, 1.
- [20] V. Coropceanu, J.-L. Brédas, S. Mehraeen, *J. Phys. Chem. C* **2017**, 121, 24954.
- [21] M. C. Heiber, C. Baumbach, V. Dyakonov, C. Deibel, *Phys. Rev. Lett.* **2015**, 3.
- [22] V. I. Arkhipov, I. A. Perova, *J. Phys. D: Appl. Phys.* **1993**, 26, 1301.
- [23] T. M. Burke, S. Sweetnam, K. Vandewal, M. D. McGehee, *Adv. Energy Mater.* **2015**, 5, 1.
- [24] A. Armin, J. R. Durrant, S. Shoaee, *J. Phys. Chem. C* **2017**, 121, 13969.
- [25] S. D. Dimitrov, S. Wheeler, D. Niedzialek, B. C. Schroeder, H. Utzat, J. M. Frost, J. Yao, A. Gillett, P. S. Tuladhar, I. McCulloch, J. Nelson, J. R. Durrant, *Nat. Commun.* **2015**, 6, 1.
- [26] F. Etzold, I. A. Howard, N. Forler, A. Melnyk, D. Andrienko, M. R. Hansen, F. Laquai, *Energy Environ. Sci.* **2015**, 8, 1511.
- [27] J. Gorenflot, M. C. Heiber, A. Baumann, J. Lorrmann, M. Gunz, V. Dyakonov, C. Deibel, *J. Appl. Phys.* **2014**, 115, 144502.
- [28] S. M. Hosseini, S. Roland, J. Kurpiers, Z. Chen, K. Zhang, F. Huang, A. Armin, D. Neher, S. Shoaee, *J. Org. Chem. C* **2019**, 123, 6823.
- [29] J. Kurpiers, D. Neher, *Sci. Rep.* **2016**, 6, 1.
- [30] D. Credgington, F. C. Jamieson, B. Walker, T.-Q. Nguyen, J. R. Durrant, *Adv. Mater.* **2012**, 24, 2135.
- [31] R. A. Marsh, J. M. Hodgkiss, R. H. Friend, *Adv. Mater.* **2010**, 22, 3672.